Acta Crystallographica Section D
Biological Crystallography
ISSN 0907-4449

Structural analysis and insights into the glycon specificity of the rice GH1 Os7BGlu26 β-D-mannosidase

Anupong Tankrathok,[a] Javier Iglesias-Fernández,[b] Sukanya Luang,[a,c] Robert C. Robinson,[d,e,f] Atsuo Kimura,[g] Carme Rovira,[b,h] Maria Hrmova[c] and James R. Ketudat Cairns[a,i]*

[a]School of Biochemistry, Institute of Science, Suranaree University of Technology, Nakhon Ratchasima 30000, Thailand, [b]Computer Simulation and Modeling Laboratory and Institut de Química Teòrica i Computacional (IQTCUB), Parc Científic de Barcelona, Baldiri Reixac 10-12, 08028 Barcelona, Spain, [c]Australian Centre for Plant Functional Genomics, School of Agriculture, Food and Wine, University of Adelaide, Glen Osmond, Australia, [d]Institute of Molecular and Cell Biology, 61 Biopolis Drive, Singapore 138673, Singapore, [e]Department of Biochemistry, National University of Singapore, 8 Medical Drive, Singapore 117597, Singapore, [f]School of Biological Sciences, Nanyang Technological University, 60 Nanyang Drive, Singapore 637551, Singapore, [g]Research Faculty of Agriculture, Hokkaido University, Sapporo, Hokkaido 060-8589, Japan, [h]Institució Catalana de Recerca i Estudis Avançats (ICREA), Passeig Lluís Companys 23, 08018 Barcelona, Spain, and [i]Laboratory of Biochemistry, Chulabhorn Research Institute, Bangkok 10210, Thailand

Correspondence e-mail: cairns@sut.ac.th

Received 17 March 2013
Accepted 24 July 2013

PDB References:
Os7BGlu26, native, 4jho; mannose complex, 4jie

Rice Os7BGlu26 is a GH1 family glycoside hydrolase with a threefold higher k_{cat}/K_m value for 4-nitrophenyl β-D-mannoside (4NPMan) compared with 4-nitrophenyl β-D-glucoside (4NPGlc). To investigate its selectivity for β-D-mannoside and β-D-glucoside substrates, the structures of apo Os7BGlu26 at a resolution of 2.20 Å and of Os7BGlu26 with mannose at a resolution of 2.45 Å were elucidated from isomorphous crystals in space group $P2_12_12_1$. The $(\beta/\alpha)_8$-barrel structure is similar to other GH1 family structures, but with a narrower active-site cleft. The Os7BGlu26 structure with D-mannose corresponds to a product complex, with β-D-mannose in the $^1S_5$ skew-boat conformation. Docking of the $^1S_3$, $^1S_5$, ^2S_O and $^3S_1$ pyranose-ring conformations of 4NPMan and 4NPGlc substrates into the active site of Os7BGlu26 indicated that the lowest energies were in the $^1S_5$ and $^1S_3$ skew-boat conformations. Comparison of these docked conformers with other rice GH1 structures revealed differences in the residues interacting with the catalytic acid/base between enzymes with and without β-D-mannosidase activity. The mutation of Tyr134 to Trp in Os7BGlu26 resulted in similar k_{cat}/K_m values for 4NPMan and 4NPGlc, while mutation of Tyr134 to Phe resulted in a 37-fold higher k_{cat}/K_m for 4NPMan than 4NPGlc. Mutation of Cys182 to Thr decreased both the activity and the selectivity for β-D-mannoside. It was concluded that interactions with the catalytic acid/base play a significant role in glycon selection.

1. Introduction

β-D-Mannosidases (β-D-mannopyranoside mannohydrolases; EC 3.2.1.25) hydrolyze β-glycosidic linkages between non-reducing β-D-mannosyl residues and the neighbouring aglycons or oligosaccharides. β-D-Mannosidases are found in a variety of organisms, including archaea, bacteria, animals, fungi and plants. In plants, these enzymes are present during and following seed germination in legumes (McCleary & Matheson, 1975), lettuce (*Lactuca sativa* L.; Ouellette & Bewley, 1986) and tomato (*Lycopersicon esculentum* Mill.; Mo & Bewley, 2002). Hrmova *et al.* (2006) showed that barley (*Hordeum vulgare* L.) β-glucosidase isoenzyme II (also called BGQ60 and βII, and designated here as HvBII), appears to work as a β-D-mannosidase in concert with β-mannanase to hydrolyze barley seed β-D-mannans; they therefore they gave it the new name HvMannos.

β-D-Mannosidases belong to glycoside hydrolase (GH) families GH1, GH2 and GH5 in CAZy (Carbohydrate-Active enZYmes Database; http://www.cazy.org; Cantarel *et al.*,

2009). These families fall within the GH-A clan, the members of which adopt a $(\beta/\alpha)_8$-barrel structure with two catalytic glutamic acid residues, the acid/base and the nucleophile, located at the C-terminal ends of β-strands 4 and 7, respectively. Currently, only two β-D-mannosidase structures have been reported, both from bacteria: GH2 Man2A from *Bacteroides thetaiotaomicron* VPI-5482 (Tailford *et al.*, 2008) and GH5 Man5A from *Cellvibrio mixtus* NCIMB 8633 (Dias *et al.*, 2004). While no GH1 β-D-mannosidase structure has yet been reported, the structures of 39 other GH1 hydrolases are available, including five from archaea, 17 from bacteria and 17 from eukaryotes, most of which represent β-D-glucosidases (EC 3.2.1.21). A few other GH1 structures represent bacterial β-D-glycosidases with broad substrate specificity: two are thioglucosidases (EC 3.2.1.147), five are 6-phospho-β-glucosidases (EC 3.2.1.86) and one is a 6-phospho-β-galactosidase (EC 3.2.1.85).

It is believed that β-D-mannosides and β-D-glucosides, which differ only in that the 2-hydroxyl group is axial in D-mannose and equatorial in D-glucose, are hydrolyzed *via* different conformational trajectories based on X-ray crystallographic (Vocadlo & Davies, 2008) and conformational free-energy landscape analysis (Biarnés *et al.*, 2007; Ardèvol *et al.*, 2010) data, as shown in Fig. 1. During hydrolysis, β-D-glucopyranosyl rings are thought to undergo a conformational change *via* a $^4H_3$ half-chair. The ring appears to be primed to form this half-chair by its distortion to a $^1S_3$ skew boat upon binding the enzyme and upon completing the glycosylation step of hydrolysis, and the glucose in the covalent glycosyl-enzyme intermediate is found in a relaxed $^4C_1$ conformation (Davies *et al.*, 1998, 2012; Fig. 1*a*). In contrast, the crystal structures of the β-D-mannosidase complexes with substrate and transition-state-based inhibitors reveal a $^1S_5$ skew boat in the Michaelis complex, which proceeds through a $B_{2,5}$ boat near the transition state to an $^OS_2$ skew boat in the covalent complex (Ducros *et al.*, 2002; Tailford *et al.*, 2008; Fig. 1*b*). The β-D-mannoside has been reported in the $^1S_5$ skew-boat conformation in Michaelis complexes with a GH2 β-mannosidase (PDB entry 2wbk; Offen *et al.*, 2009) and a GH26 β-mannanase (PDB entry 1gvy; Ducros *et al.*, 2002). The $^1S_3$ skew-boat conformation of β-D-glucoside substrates has been reported in several enzymes, including the GH1 sorghum dhurrinase (PDB entry 1v03; Verdoucq *et al.*, 2004), rice (*Oryza sativa*) Os3BGlu6 (PDB entry 3gnp; Seshadri *et al.*, 2009), termite (*Neotermes koshunensis*) β-D-glucosidase *NK*Bgl (PDB entry 3ai0; Jeng *et al.*, 2011) and rice Os4BGlu12 (PDB entry 3ptq; Sansenya *et al.*, 2011). In the case of rice BGlu1 (designated here with its systematic name Os3BGlu7), the nonreducing β-D-glucopyranosyl ring in the oligosaccharide complexes with catalytic mutants was reported to be between the $^1S_3$ and $^4H_3$ or closely related ^4E conformations, again supporting the trajectory of $^1S_3$ to $^4H_3$ (Chuenchor *et al.*, 2011). Calculations of the energetics of the conformational transitions in solution show the same conformational preferences of $^1S_3$ to $^4H_3$ to $^4C_1$ for β-D-glucosides and $^1S_5$ to $B_{2,5}$ to $^OS_2$ for β-D-mannosides, suggesting that the enzymes may tend to bind the lowest energy forms as they catalyze hydrolysis (Biarnés *et al.*, 2007; Ardèvol *et al.*, 2010).

Plant β-D-mannosidases fall into a single amino-acid sequence-based phylogenetic cluster of GH1, which also contains β-D-glucosidases with β-D-mannosidase activity (Opassiri *et al.*, 2006; Kuntothom *et al.*, 2009). The amino-acid sequences of rice Os7BGlu26 and three closely related rice β-D-glycosidase isoenzymes (Os3BGlu7, Os1BGlu1 and Os3BGlu8) are grouped into this phylogenetic cluster with the barley HvBII (Hrmova *et al.*, 1996, 1998), *Arabidopsis* BGLU44 (Xu *et al.*, 2004) and tomato LeMside (Mo & Bewley, 2002) β-D-mannosidases, with which Os7BGlu26 shares 82, 66 and 66% amino-acid sequence identity, respectively (Opassiri *et al.*, 2006; Kuntothom *et al.*, 2009). Within this group, only Os3BGlu7 has an elucidated structure, but it hydrolyzes 4NPGlc with a 34-fold higher k_{cat}/K_m value than 4NPMan (Opassiri *et al.*, 2004). In contrast, rice Os7BGlu26

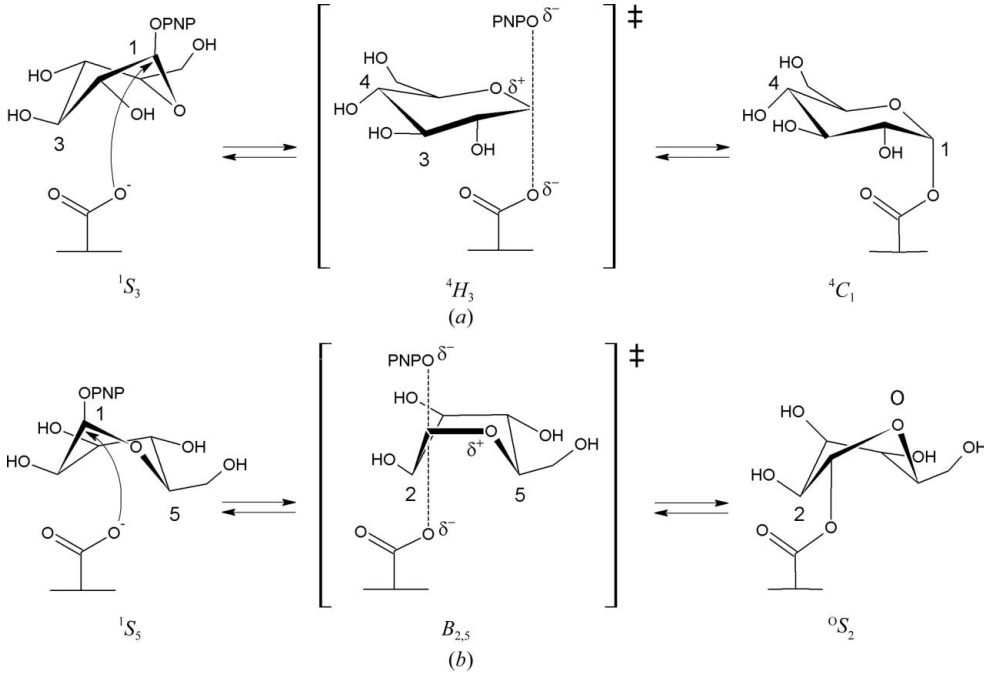

Figure 1
A proposed pyranose-ring itinerary of β-D-glucosides (*a*) and β-D-mannosides (*b*) during the glycosylation step of the hydrolytic pathway (Davies *et al.*, 2003; Vocadlo & Davies, 2008).

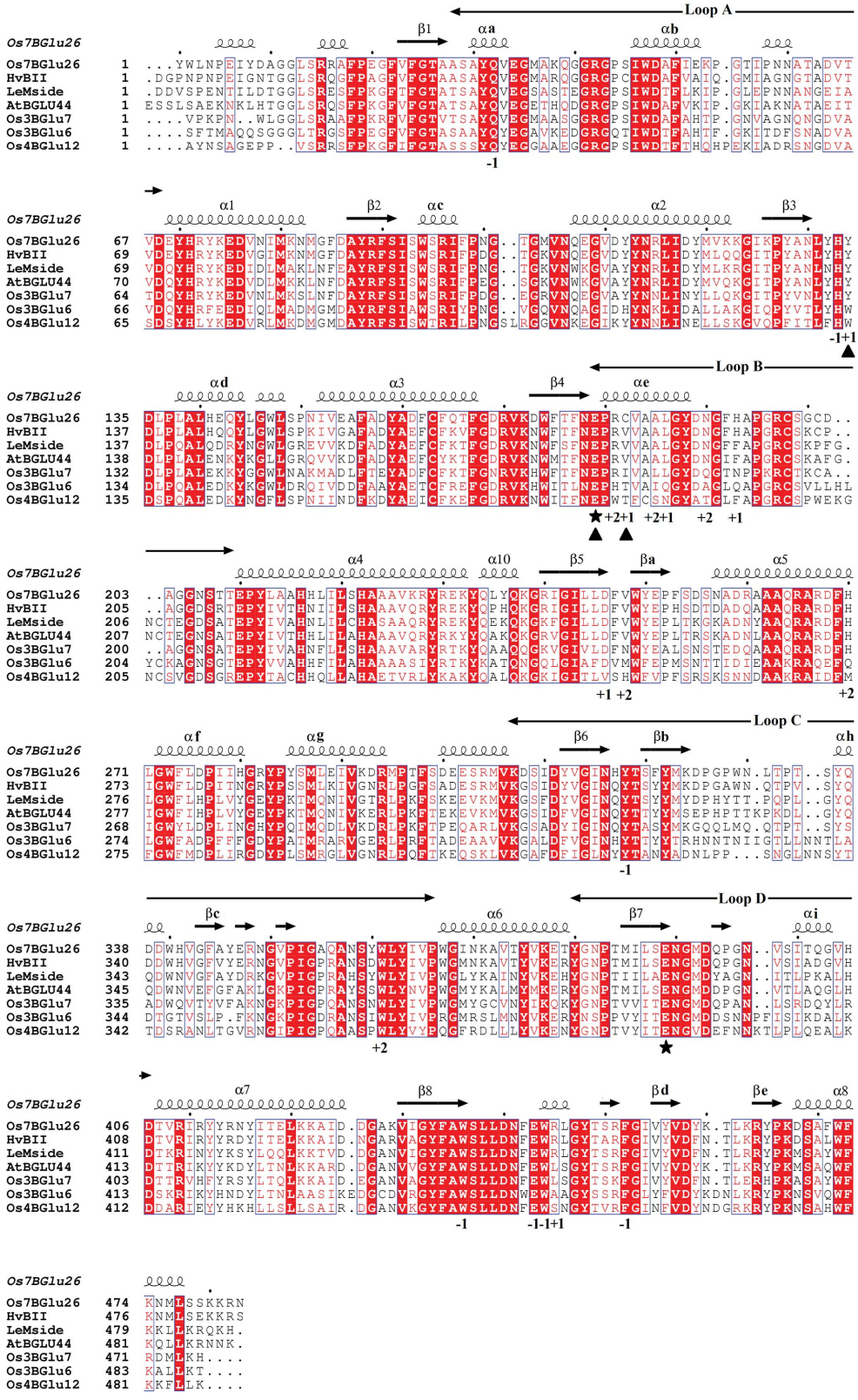

Figure 2
Multiple sequence alignment of rice Os7BGlu26, HvBII, LeMside, AtBGlu44, Os3BGlu7, Os3BGlu6 and Os4BGlu12. The amino-acid sequences were aligned with *ClustalW* and the secondary structure of Os7BGlu26 was aligned at the top of the alignment with *ESPript* (Gouet *et al.*, 2003). Stars indicate the catalytic acid/base and nucleophilic residues, while black arrowheads mark the amino-acid residues that were mutated in this study. The GenBank accession codes for the sequences are Os7BGlu26, ACF35791; HvBII, AAA87339; LeMside, AAL37714; AtBGLU44, Q9LV33; Os3BGlu7, AC091670; Os3BGlu6, AC146619; Os4BGlu12, AAAA02014151.

and barley HvBII, which have closely related amino-acid sequences, as shown in Fig. 2, hydrolyze 4NPMan with three-fold and 12-fold higher k_{cat}/K_m values than 4NPGlc, respectively (Kuntothom *et al.*, 2009). The Os7BGlu26 β-D-mannosidase also hydrolyzes mannooligosaccharides and cellooligosaccharides and the natural glycosides dhurrin, D-amygdalin and *p*-coumaryl alcohol β-D-glucoside.

Given the difference observed in the hydrolysis of the glucoside and mannoside substrates, it is of interest to understand the basis of β-D-mannosidase catalysis in GH1 enzymes that have both β-D-mannosidase and β-D-glucosidase activities and their preference for β-D-mannoside *versus* β-D-glucoside substrates. Saturation transfer difference nuclear magnetic resonance (STD-NMR) showed HvBII β-D-mannosidase bound 4NP β-D-thioglucoside in either a $^{1}S_{3}$ or $^{3}S_{5}$ conformation and 4NP β-D-thiomannoside in a relaxed $^{4}C_{1}$ chair (Kuntothom *et al.*, 2010). Quantum mechanics/molecular mechanics (QM/MM) simulations for Os3BGlu7 β-D-glucosidase and HvBII β-D-mannosidase binding indicated their preference to bind $^{1}S_{3}$ skew-boat conformations of 4NPGlc, 4NPMan and 4-nitrophenyl β-D-thiomannoside and the $^{4}C_{1}$ chair conformation of β-D-thioglucoside in the Michaelis complex. Notably, Kuntothom *et al.* (2010) used a homology model of the HvBII β-D-mannosidase in the QM/MM simulations, owing to the lack of a GH1 β-D-mannosidase structure. To investigate the molecular mechanism of β-D-mannosidase specificity in plant GH1 β-D-mannosidases, we determined the crystal structure of Os7BGlu26 β-D-mannosidase and probed the residues involved by computational docking and mutagenesis.

Table 1
Data-collection and processing statistics.

Values in parentheses are for the outer shell.

	Native Os7BGlu26	Os7BGlu26–mannose complex
PDB code	4jho	4jie
Wavelength (Å)	1.00	1.00
Resolution range (Å)	30–2.20 (2.28–2.20)	30–2.45 (2.54–2.45)
Completeness (%)	99.9 (99.9)	95.8 (79.9)
Average multiplicity per shell	5.5 (5.5)	6.1 (4.4)
$R_{\rm merge}$† (%)	8.8 (49.4)	14.9 (45.6)
$\langle I/\sigma(I)\rangle$	18.0 (3.2)	11.9 (3.2)
Space group	$P2_12_12_1$	$P2_12_12_1$
Unit-cell parameters (Å)	a = 68.1, b = 71.7, c = 136.7	a = 68.0, b = 73.6, c = 134.0
No. of unique reflections	34370	24116
No. of observed reflections	188040	147585
No. of molecules per asymmetric unit	1	1
R factor (%)	17.6	15.3
$R_{\rm free}$‡ (%)	21.9	19.5
No. of protein atoms	3955	3960
No. of water molecules	305	234
No. of ligand atoms	0	12
No. of non-solvent heteroatoms	51	51
R.m.s.d., bonds (Å)	0.010	0.010
R.m.s.d., angles (°)	1.155	1.212
Mean B factor (Å^2)		
Protein	22.9	23.7
Non-solvent heteroatoms	45.0	46.9
Solvent	32.8	30.8
D-Mannose	—	31.4
Ramachandran plot, residues in (%)		
Most favoured region	88.5	88.0
Allowed region	11.3	11.7
Outlier region	0.2	0.2

† $R_{\rm merge} = \sum_{hkl}\sum_i |I_i(hkl) - \langle I(hkl)\rangle| / \sum_{hkl}\sum_i I_i(hkl)$. ‡ $R_{\rm free}$ represents the residual factor calculated from approximately 5% of the data that were not used in the refinement.

2. Materials and methods

2.1. Protein expression and purification

The pET32a/Os7BGlu26 plasmid, which includes the *Os7BGlu26* cDNA in frame to produce an N-terminally thioredoxin and His-tagged Os7BGlu26 fusion protein (Kuntothom *et al.*, 2009), was transformed into *Escherichia coli* strain Rosetta-gami(DE3) cells. The cells were cultured in low-salt LB (Lennox) medium containing 50 µg ml^{-1} ampicillin, 15 µg ml^{-1} kanamycin, 12.5 µg ml^{-1} tetracycline and 34 µg ml^{-1} chloramphenicol. When the optical density at 600 nm of the culture reached 0.4–0.5, protein expression was induced with 0.3 m*M* IPTG for 24 h at 293 K. The cell pellets were collected by centrifugation and suspended in extraction buffer [50 m*M* Tris–HCl pH 8.0, 150 m*M* sodium chloride, 200 µg ml^{-1} lysozyme, 1%(*v*/*v*) Triton X-100, 1 m*M* PMSF, 4 µg ml^{-1} DNase I] at approximately 298 K for 30 min. Insoluble debris was removed by centrifugation and the protein was purified from the soluble extract by immobilized metal-affinity chromatography (IMAC) on cobalt-equilibrated IMAC resin (GE Healthcare). The resin was washed with equilibration buffer (150 m*M* NaCl, 50 m*M* Tris–HCl pH 8.0) followed by 20 m*M* imidazole in equilibration buffer and was eluted with 250 m*M* imidazole in equilibration buffer. The fractions of Os7BGlu26 containing β-D-glucosidase activity, as judged by 4NPGlc hydrolysis, were pooled and imidazole was removed by dialysis in 150 m*M* NaCl, 20 m*M* Tris–HCl buffer pH 8.0. The dialysed preparation was concentrated in a 30 kDa molecular-weight cutoff (MWCO) Centricon centrifugal filter (Millipore). The N-terminal fusion tag was removed from the Os7BGlu26 fusion protein by cleavage with 2 ng enterokinase (New England Biolabs) per milligram of fusion protein at 296 K for 18 h followed by a second round of IMAC. The flowthrough fractions containing β-glucosidase activity were pooled and the protein purity was analysed by SDS–PAGE. The Os7BGlu26 was dialysed and concentrated with a 30 kDa MWCO Centricon filter to obtain Os7BGlu26 protein at approximately 6 mg ml^{-1} in 50 m*M* NaCl, 20 m*M* Tris–HCl buffer pH 8.0.

2.2. Protein crystallization

Before crystallization, purified Os7BGlu26 was filtered through an Ultrafree-MC 0.22 µm filter (Millipore; 4000*g*, 277 K, 5 min). Crystallization conditions were screened by the microbatch-under-oil method at 288 K with precipitants from the Crystal Screen HT kit (Hampton Research). After optimization of the crystallization conditions, the crystals were grown in 0.8 *M* potassium/sodium tartrate, 0.1 *M* Na HEPES pH 7.5. For the complex with ligand, the crystals were soaked in 400 m*M* D-mannose in the precipitant solution. Prior to data collection, the crystals were soaked in cryoprotectant containing the precipitant, 400 m*M* D-mannose and 20%(*v*/*v*) glycerol. The crystals were flash-vitrified and stored in liquid nitrogen.

2.3. Data collection, processing and structure refinement

The X-ray data for Os7BGlu26 were collected on the BL13B1 beamline at the National Synchrotron Radiation Research Center (NSRRC), Hsinchu, Taiwan using a 1.0 Å wavelength X-ray beam and an ADSC Quantum 315 CCD detector. The crystals were maintained at 110 K in a cold stream of nitrogen throughout data collection. All data sets were indexed, integrated and scaled with the *HKL*-2000 package (Otwinowski & Minor, 1997). The native structure was solved by molecular replacement with the rice Os3BGlu7 β-glucosidase structure (PDB entry 2rgl; Chuenchor *et al.*, 2008) as a search model and *MOLREP* (Vagin & Teplyakov, 2010) in the *CCP*4 suite of programs (Winn *et al.*, 2011) followed by refinement with *REFMAC*5 (Murshudov *et al.*, 2011). The structure of the complex with D-mannose was solved by rigid-body refinement of the native structure in *REFMAC*5. Model building was performed with *Coot* (Emsley & Cowtan, 2004). For the Os7BGlu26–mannose complex structure, initial refinement and model building was performed with a resolution cutoff of 2.25 Å. However, owing to the low completeness of the refined data in the outer shells, the model was refined to a 2.45 Å cutoff to achieve acceptable completeness parameters (Table 1). The quality of the final model was assessed with *PROCHECK* (Laskowski *et al.*, 1993)

and *MolProbity* (Chen *et al.*, 2010). Graphic representations of structures were generated in *PyMOL* (Schrödinger LLC).

2.4. Docking calculations

The 4NPMan and 4NPGlc ligands were docked into the active site of Os7Glu26 *via* a Lamarckian genetic search algorithm as implemented in *AutoDock* 4.2 (Morris *et al.*, 2009). The ligands were docked in four different conformations ($^1S_3$, $^1S_5$, ^2S_O and $^3S_1$), which are representative of the different catalytic itineraries followed by glycoside hydrolases (Vocadlo & Davies, 2008). The ligand conformations were constructed manually by adding the 4NP portion to the corresponding sugar conformations obtained from previous studies (Biarnés *et al.*, 2007; Ardèvol *et al.*, 2010). All ligands were geometry optimized with density functional theory and *CPMD* (v.3.15; CPMD Consortium; http://www.cpmd.org/). A restraint on the sugar ring was added to maintain the desired conformation. All calculations were performed on the Os7BGlu26 enzyme excluding all crystallographic water molecules. The protonation states of histidine residues were assigned based on the hydrogen-bond environment and Glu179 was modelled as protonated because of its role as an acid/base residue. Gasteiger charges were assigned to the protein and ligand atoms using *AutoDockTools*. 100 *AutoDock* runs were performed for each of the substrates tested to calculate the binding energy, holding the enzyme but not the ligands fixed. A grid with dimensions of 40 × 40 × 40 Å centred on the catalytic acid/base (Glu179) and nucleophile (Glu389) residues was used.

2.5. Site-directed mutagenesis

Os7BGlu26 mutants were constructed using the QuikChange site-directed mutagenesis kit (Stratagene) with the pET32a/Os7BGlu26 plasmid as the template. The following oligonucleotide primers were used for mutagenesis: for the E179Q mutation, 5′-GAC TGG TTT ACC TTC AAT **C**AG CCG AGA TGC GTT GCT G-3′ and its reverse complement; for Y134W, 5′-GCA AAC CTC TAC CAC T**GG** GAC CTA CCA TTA GCA C-3′ and its reverse complement; for C182T, 5′-CTT CAA TGA GCC GAG A**AC** CGT TGC TGC TCT AGG-3′ and its reverse complement; for Y134F, 5′-CGC AAA CCT CTA CCA CT**T** TGA CCT ACC ATT AGC AC-3′ and its reverse complement; for C182A, 5′-CTT CAA TGA GCC GAG A**GC** CGT TGC TGC TCT AGG-3′ and its reverse complement (the mutated bases are shown in bold in each case). All mutant plasmids were sequenced through the entire Os7BGlu26 coding region in both directions.

2.6. Kinetic studies

The kinetic parameters of the enzymes with the 4NPGlc and 4NPMan substrates were determined from triplicate assays containing 0.05–18.5 µg enzyme, substrates at concentrations from 0.01 to 30 m*M* and 1 µg µl^{-1} BSA in 50 m*M* sodium acetate buffer pH 5.0, in a total volume of 140 µl, at 303 K for reaction intervals that had linear initial velocities (pseudo-first-order rate or V_o). Reactions were stopped by alkalinization with 70 µl 0.4 *M* sodium carbonate and the absorbance at 405 nm was read and compared with a 4-nitrophenolate standard curve in the same buffer. The kinetic parameters were calculated by nonlinear regression of the Michaelis–Menten plots with *GraFit* 5.0 (Erithacus Software, Horley, Surrey, England). The Gibbs free-energy change of transition-state binding was calculated as $\Delta\Delta G_{S^*mut} = -RT[\ln(k_{cat}/K_m)_{mutant} - \ln(k_{cat}/K_m)_{wild\ type}]$ (Fersht *et al.*, 1987). The inhibition constant (K_i) of Os7BGlu26 for inhibition by HEPES was determined at 303 K by incubating 2 µg enzyme in 50 m*M* sodium acetate buffer pH 5.0 containing 1 µg µl^{-1} BSA with 0–300 m*M* HEPES for 10 min. The residual enzyme activities were monitored by assaying the activity towards 0.1, 0.5, 1.0 and 1.5 m*M* 4NPMan. Inhibition constants K_i were calculated by linear regression of a plot of the apparent K_m/V_{max} values (slopes of Lineweaver–Burk plots) *versus* inhibitor concentrations.

3. Results and discussion

3.1. Os7BGlu26 protein and crystal production

The expression of the soluble 66 kDa Os7BGlu26 fusion protein with N-terminal thioredoxin and His tags was improved in *E. coli* strain Rosetta-gami(DE3) compared with the previously reported expression of the same construct in the Origami(DE3) strain (Kuntothom *et al.*, 2009). Purification by IMAC, followed by removal of the N-terminal fusion tag by enterokinase cleavage and adsorption of the tag to IMAC resin, yielded the 50 kDa Os7BGlu26 protein with approximately 90% purity on SDS–PAGE (Supplementary Fig. S1[1]). This protein was screened for crystallization and Os7BGlu26 crystals with dimensions of 90 × 20 × 20 µm were observed within one week in microbatch screening with a precipitant consisting of 0.8 *M* potassium/sodium tartrate, 0.1 *M* Na HEPES pH 7.5. When the pH and salt concentrations of the precipitant were optimized in hanging-drop vapour diffusion, a single crystal with dimensions of 160 × 25 × 25 µm was obtained within 5 d in 0.58 *M* potassium/sodium tartrate, 0.1 *M* Na HEPES pH 7.25 (Supplementary Fig. S2).

3.2. Structure and model quality

The apo Os7BGlu26 crystal diffracted X-rays to 2.20 Å resolution and belonged to the orthorhombic space group $P2_12_12_1$. Its unit-cell parameters were a = 68.1, b = 71.7, c = 136.7 Å. Diffraction of the crystal soaked in D-mannose gave an isomorphous data set that was processed to 2.45 Å resolution with unit-cell parameters a = 68.0, b = 73.6, c = 134.0 Å. The data-collection statistics for both crystals are summarized in Table 1. The asymmetric units of both crystals were estimated to contain one molecule, with a Matthews coefficient (V_M) of 3.03 Å^3 Da^{-1} (Matthews, 1968) and a solvent content of 59.5% for the apo Os7BGlu26 crystal and

[1] Supplementary material has been deposited in the IUCr electronic archive (Reference: DW5051). Services for accessing this material are described at the back of the journal.

a V_M of 3.05 Å^3 Da^{-1} and a solvent content of 59.7% for the D-mannose-soaked crystal.

The fold of the structure of Os7BGlu26 is a classic TIM $(\beta/\alpha)_8$-barrel, similar to other GH1 enzymes (Fig. 3*a*). The structure placed the highly conserved Glu179 and Glu389 at the C-terminal ends of β-strands 4 and 7, respectively. These residues are positioned at the bottom of the active-site cleft, as observed for the catalytic acid/base and nucleophile residues in other members of GH clan A (Jenkins *et al.*, 1995; Henrissat *et al.*, 1995). Furthermore, nucleophilic rescue of mutants of the corresponding residues confirmed that they are the catalytic residues in the closely related Os3BGlu7 β-D-glucosidase (Hommalai *et al.*, 2007; Chuenchor *et al.*, 2011). The four variable loops that have been reported to account for much of the GH1 structural and functional diversity (Sanz-Aparicio *et al.*, 1998) connect the β-strands and α-helices at the carboxy-terminal side of the core barrel structure. These loops are loop A (Ala28–Asp68), loop B (Glu179–Thr209), loop C (His317–Pro366) and loop D (Asn390–Asp406) (Figs. 2 and 3*a*). Although no electron density was observed for the 14 residues from the N-terminal fusion tag (A-M-A-D-I-T-S-L-Y-K-K-A-G-S-A) and the five C-terminal residues (S-K-K-R-N), five amino-acid residues of the fusion-protein linker region (A-A-P-F-T) and residues 1–478 of the mature Os7BGlu26 gave clear electron density for the structure. Two *cis*-peptide bonds were found between Ala194 and Pro195 and between Trp436 and Ser437, as seen in other plant GH1 enzymes (Barrett *et al.*, 1995). The conserved disulfide bond found in nearly all plant GH1 enzymes was present in loop B between Cys198 and Cys201. The conserved active-site tryptophan, Trp444, fell in the outlier region of the Ramachandran plot, while it is found in a similar outlier or borderline region in other GH1 enzymes (Czjzek *et al.*, 2000; Chuenchor *et al.*, 2008). The other Ramachandran statistics were similar to those of other plant GH1 structures.

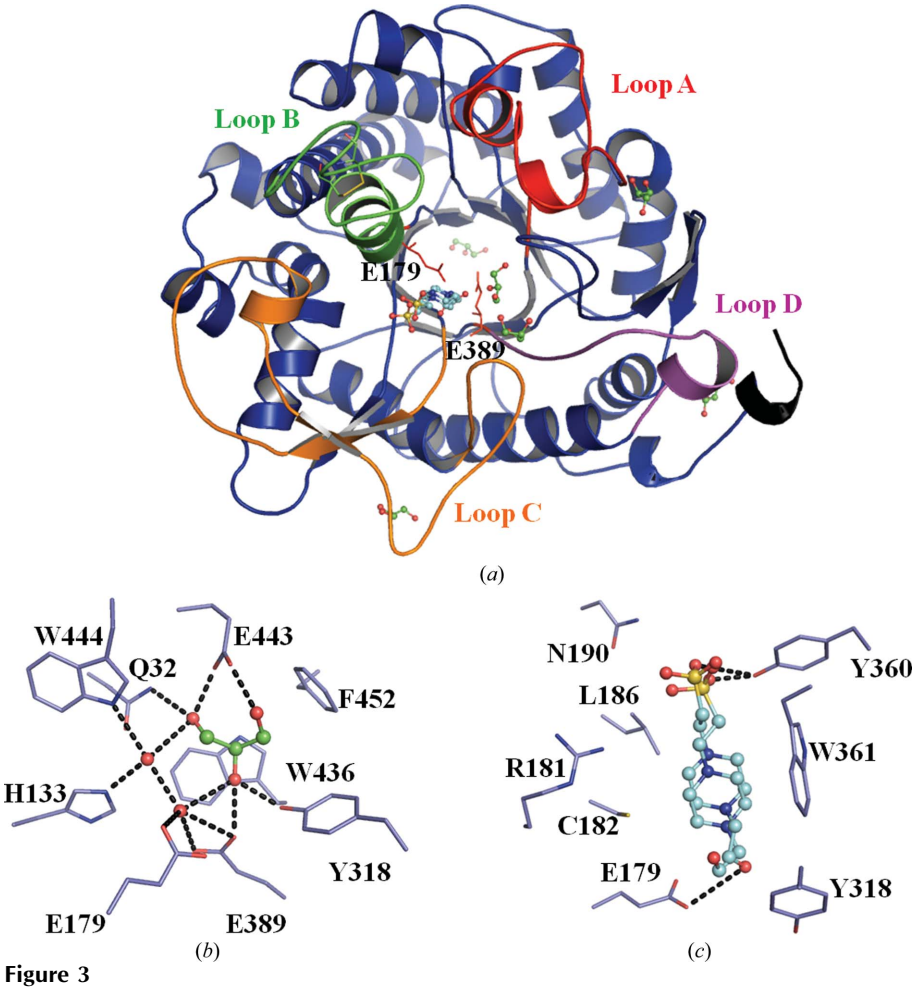

Figure 3
Structure of rice Os7BGlu26 β-D-mannosidase. (*a*) Cartoon representation of the overall structure of rice Os7BGlu26. The catalytic nucleophile and acid/base residues are represented as red sticks (Glu389 and Glu179); glycerol and HEPES are shown as green and cyan ball-and-stick representations, respectively. Loops A, B, C and D are indicated in red, green, orange and magenta, respectively. The N-terminus is indicated in black. (*b*) Amino-acid residues around the −1 subsite with contacts mediated through hydrogen bonds that cover distances of between 2.4 and 3.1 Å and are indicated as black dashed lines. (*c*) Amino-acid residues interacting with the HEPES molecule in two alternate positions in the active site. The contacts through hydrogen bonds between the protein and HEPES are indicated as black dashed lines.

Fig. 3(*b*) shows that a glycerol molecule originating from the cryoprotectant was bound in the active site. This molecule hydrogen-bonded to Gln32, Tyr318, Glu389, Glu443 and two water molecules, which also interacted with His133 and Trp444 and the catalytic residues Glu179 and Glu389. The distance between the C^δ atoms of the catalytic acid/base Glu179 and the nucleophile Glu389 was 4.9 Å, which is consistent with the distance expected for the retaining mechanism of glycoside hydrolases (Rye & Withers, 2000). The carboxyl O atom of Glu179, the acid/base residue, made a close contact of 2.7 Å with the Tyr134 hydroxyl. In addition, the conserved Trp436 and Phe452 residues at the −1 subsite provided an aromatic platform for sugar binding and additional hydrophobic interactions with the substrate, respectively (Figs. 3*b* and 3*c*), as noted for other GH1 enzymes (Czjzek *et al.*, 2000). A HEPES molecule from the crystallization buffer was found in the substrate-binding cleft at the +1, +2 and +3 subsites, which were defined for the binding of β-(1,4)-linked D-glucosyl residues in Os3BGlu7 (Chuenchor *et al.*, 2011). The HEPES molecule was most favourably modelled in two alternate conformations, both of which hydrogen-bonded to Glu179 and Tyr360 (Fig. 3*c*). HEPES was found to bind to Os7BGlu26 with a non-competitive inhibition constant K_i of 81.4 m*M* and $\Delta G = -6.3$ kJ mol^{-1} (Supplementary Fig. S3). The combined occupancy of

the two alternate HEPES molecules was constrained to be 1.0 in the refinement. This artificial full occupancy is reflected by higher temperature factors (B = 28.9–46.4 Å^2 for the individual HEPES atoms; Table 1).

3.3. Structural comparison of Os7BGlu26 with other rice GH1 structures

In comparison to other rice GH1 structures, the active site of Os7BGlu26 has the narrowest shape, with a gate of 9.9 × 12.5 Å (from the atom centres of Gln337 O$^{\varepsilon1}$ to Tyr360 O$^{\eta}$ and of Asn190 N$^{\varepsilon2}$ to Tyr346 O$^{\eta}$, respectively) owing to the presence of Phe192 on loop B and Tyr360 on loop C, which constrict the substrate route into the active site. In comparison, these parameters for the Os3BGlu7 (10.3 × 18.1 Å from Gln187 C$^{\delta}$ to Trp358 C$^{\beta}$ and from Tyr341 C$^{\varepsilon2}$ to Leu442 C$^{\beta}$, respectively), Os3BGlu6 (12.1 × 20.8 Å from Ala189 C$^{\beta}$ to Trp366 C$^{\beta}$ and from Leu342 C$^{\delta2}$ to Ala454 C$^{\alpha}$, respectively) and Os4BGlu12 (10.1 × 19.8 Å from Lys203 C$^{\varepsilon}$ to Trp365 C$^{\beta}$ and from Leu348 C$^{\delta1}$ to Asn452 C$^{\alpha}$, respectively) β-D-glucosidases indicate that these enzymes have broader substrate-binding clefts (Fig. 4). This suggests that the preferred substrate for Os7BGlu26 should be one with a small aglycon or a straight- and narrow-chain oligosaccharide, consistent with its hydrolysis of β-(1,4)-linked manno-oligosaccharides and gluco-oligosaccharides, dhurrin, D-amygdalin and p-coumaryl alcohol glucoside (Supplementary Fig. S4; Kuntothom *et al.*, 2009).

Although the four rice GH1 enzymes have different substrate specificities, their overall structures are very similar. Upon superposition of these structures, Os7BGlu26 had an r.m.s.d. value of 0.576 Å over 437 C$^{\alpha}$ atoms with rice Os3BGlu7 β-glucosidase (PDB entry 2rgl; Chuenchor *et al.*, 2008), with which it shares 63% sequence identity. The other r.m.s.d. values are 0.481 Å over 379 C$^{\alpha}$ residues with Os3BGlu6 (PDB entry 3gno; 52% sequence identity; Seshadri *et al.*, 2009), and 0.522 Å over 391 C$^{\alpha}$ residues with Os4BGlu12 (PDB entry 3ptk; 51% sequence identity; Sansenya *et al.*, 2011).

3.4. Os7BGlu26 in complex with the D-mannose hydrolysis product

To provide evidence for the interactions between Os7BGlu26 and D-mannosyl glycon, D-mannose was soaked into the Os7BGlu26 crystal. The resolution of the data set for this complex was limited to 2.45 Å, which resulted in a calculated $F_o - F_c$ OMIT map in which the mannose residue could be placed unambiguously (Fig. 5*a*). The density clearly showed the presence of D-mannose in the β-anomeric configuration and the $^1S_5$ conformation, indicating that Os7BGlu26 specifically binds the β-anomer of D-mannose. The β-D-mannose hydrogen-bonded to Gln32, His133, Tyr134, Asn178, Glu179, Glu389, Tyr318, Glu443 and Trp444 (Fig. 5*b*).

Previous structures of β-D-mannosidase from GH2 and β-D-mannanase from GH26 include Michaelis complex, transition-state analogue and covalent intermediate complexes; however, this is the first report of a product complex. Free D-mannose in the active site of Os7BGlu26 was distorted to the $^1S_5$ skew boat, which is the same conformation as that reported for the Michaelis complexes of enzymes hydrolyzing β-D-mannosides (Ducros *et al.*, 2002; Offen *et al.*, 2009). Superposition of the β-D-mannose complex and native structures showed that the

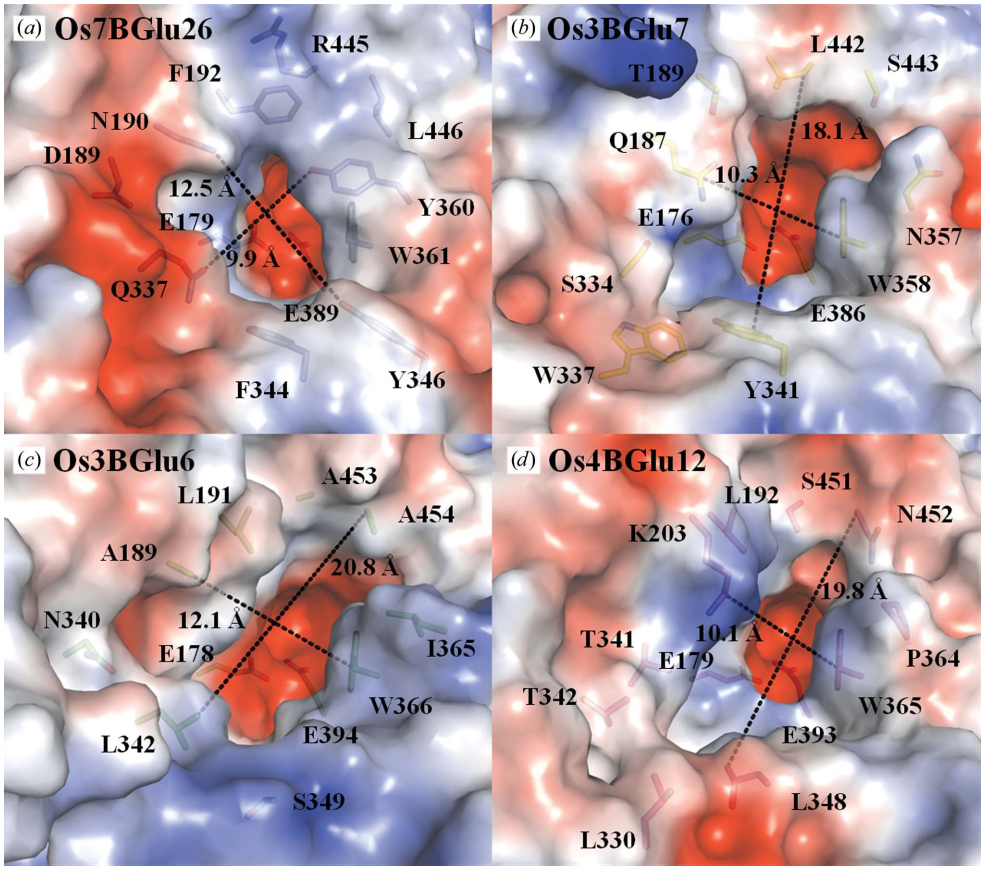

Figure 4
Comparison of the active-site clefts of the rice GH1 structures Os7BGlu26, OS3BGlu7 (PDB entry 2rgl), Os3BGlu6 (PDB entry 3gno) and Os4BGlu12 (PDB entry 3ptk). The dashed lines indicate the width and breadth of the substrate-binding cleft at the entrance to the active site, as described in the main text. *PyMOL* was used to generate qualitative vacuum electrostatic charges to colour the surfaces red for negatively charged areas and blue for positively charged areas.

β-D-mannose was in essentially the same position as the glycerol and water molecules in the native Os7BGlu26 structure (Fig. 5*c*). Nearly all of the residues in the −1 subsite were in the same positions in the two structures, with C^{δ} of the catalytic nucleophile Glu389 displaced by 0.4 Å. Superimposition of the Os7BGlu26–β-D-mannose complex structure with that of the complex of Os3BGlu7 with cellopentaose (PDB entry 3f5k; Chuenchor *et al.*, 2011) showed that the $^{1}S_{5}$-configured 1-β-D-mannose orientation was similar to that of the $^{1}S_{3}$-configured nonreducing terminal β-D-glucosyl ring of the cellopentaose in the −1 subsite. A HEPES molecule occupied the +1, +2 and +3 subsites defined for β-(1,4)-linked glucosyl residues in the Os3BGlu7 cellopentaose complex, apparently in multiple conformational states (Fig. 5*d*). This structure indicates that the β-D-mannose hydrolysis product may be retained in the −1 subsite in a $^{1}S_{5}$ conformation that suggests a conformational pathway of $^{O}S_{2}$ to $B_{2,5}$ to $^{1}S_{5}$ for the deglycosylation step of Os7BGlu26 β-D-mannoside hydrolysis, since the deglycosylation step in the retaining mechanism is essentially the reverse of the glycosylation step shown in Fig. 1.

3.5. Docking studies of the Michaelis complex

To provide further evidence for the conformational itinerary in the glycosylation step of Os7BGlu26, 4NPGlc and 4NPMan were computationally docked into the active site of the Os7BGlu26 structure in the four starting conformations observed for pyranoside rings in glycoside hydrolase mechanisms (Vocadlo & Davies, 2008). The predicted binding energies for all the conformations tested are shown in Fig. 6(*c*). The binding energies for the 4NPGlc conformations are higher

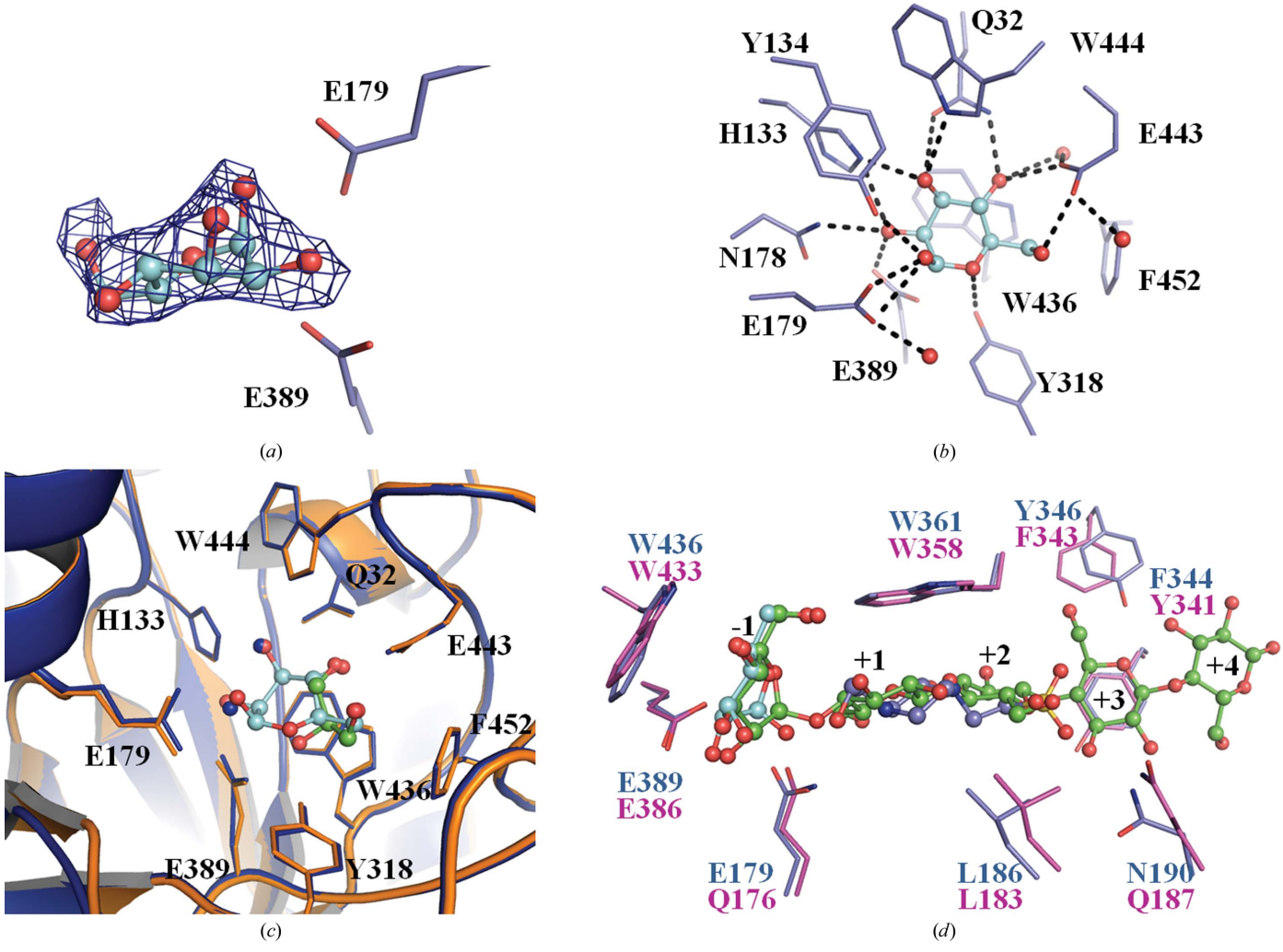

Figure 5
The structure of rice Os7BGlu26 in complex with β-D-mannose. (*a*) An unbiased $F_{o} - F_{c}$ (OMIT) map of β-D-mannose is represented as a blue mesh contoured at 3σ. (*b*) Amino-acid residues interacting with β-D-mannose in the active site. The contacts through hydrogen bonds between the protein and β-D-mannose are indicated by black dashed lines, while β-D-mannose is shown in a cyan ball-and-stick representation. The superimposition of the Os7BGlu26–β-D-mannose complex (orange) on the native Os7BGlu26 structure (blue) is shown in (*c*). The superimposition of the Os7BGlu26–β-D-mannose complex (C atoms in blue) with the Os3BGlu7 cellopentaose complex (C atoms in violet) is shown in (*d*). β-D-Mannoside, HEPES and cellopentaose are indicated in ball-and-stick representation, with C atoms in cyan, blue and green, respectively. The glucosyl residue-binding subsites observed in the Os3BGlu7 cellopentaose complex are labelled −1, +1, +2, +3 and +4.

Table 2
Kinetic parameters of wild-type Os7BGlu26 and its mutants using the substrates 4NPMan and 4NPGlc.

	Substrate	K_m (mM)	k_{cat} (s^{-1})	k_{cat}/K_m (s^{-1} mM^{-1})	Mutant/wild type k_{cat}/K_m ratio	$\Delta\Delta G_{S^*mut}$† (kJ mol^{-1})
Wild type	4NPMan	0.48 ± 0.003	0.35 ± 0.004	0.714		
	4NPGlc	0.124 ± 0.002	0.029 ± 0.0001	0.237		
E179Q	4NPMan	0.40 ± 0.003	0.008 ± 0.0004	0.02	0.028	+9.0
	4NPGlc	1.07 ± 0.02	0.0102 ± 0.0004	0.0095	0.040	+8.1
Y134W	4NPMan	2.37 ± 0.04	2.4 ± 0.09	1.01	1.4	−0.9
	4NPGlc	0.032 ± 0.002	0.0306 ± 0.0006	0.959	4.0	−3.5
C182T	4NPMan	12.4 ± 0.78	0.51 ± 0.03	0.043	0.060	+7.1
	4NPGlc	3.7 ± 0.14	0.078 ± 0.005	0.021	0.089	+6.1
Y134W/C182T	4NPMan	11.56 ± 1.70	0.30 ± 0.03	0.026	0.036	+8.3
	4NPGlc	2.95 ± 0.17	0.058 ± 0.005	0.0198	0.084	+6.3
Y134F	4NPMan	0.45 ± 0.02	12.5 ± 0.6	27.7	39	−9.2
	4NPGlc	0.167 ± 0.009	0.127 ± 0.003	0.759	3.2	−2.9
C182A	4NPMan	2.46 ± 0.23	1.02 ± 0.07	0.414	0.58	+1.4
	4NPGlc	1.39 ± 0.11	0.242 ± 0.016	0.174	0.73	+0.8

† $\Delta\Delta G_{S^*mut} = -RT[\ln(k_{cat}/K_m)_{mutant} - \ln(k_{cat}/K_m)_{wild\ type}]$ (Fersht *et al.*, 1987).

(more negative) than those calculated for 4NPMan (Fig. 6). Therefore, the glucose derivative molecule binds more tightly to the enzymatic cavity than the mannose derivative. This is consistent with the lower K_m values observed for β-D-glucoside (K_m = 0.124 mM) compared with β-D-mannoside (K_m = 0.48 mM) (Table 2).

Both 4NPMan and 4NPGlc show similar trends in binding affinity with respect to the sugar conformation (Fig. 6). However, whereas 4NPGlc binds preferentially to the enzyme in a $^1S_3$ conformation (consistently with the experimental and theoretical evidence for a $^1S_3$–$^4H_3$–$^4C_1$ catalytic conformational itinerary for β-glucosyl hydrolases), both $^1S_3$ and $^1S_5$ have a similar stability for 4NPMan. Together with the extensive literature supporting that the hydrolysis of β-D-mannosides follows a $^1S_5$–$B_{2,5}$–$^OS_2$ itinerary (Ducros *et al.*, 2002; Tailford *et al.*, 2008; Offen *et al.*, 2009; Ardèvol *et al.*, 2010), the results obtained suggest that the two substrates might follow different conformational itineraries for catalysis ($^1S_3$–$^4H_3$–$^4C_1$ for 4NPGlc and $^1S_5$–$B_{2,5}$–$^OS_2$ for 4NPMan). In fact, the $^1S_5$ mannoside substrate was found more frequently than the $^1S_3$ glucoside substrate in the docking calculations, which may explain the tenfold higher k_{cat} observed for the former.

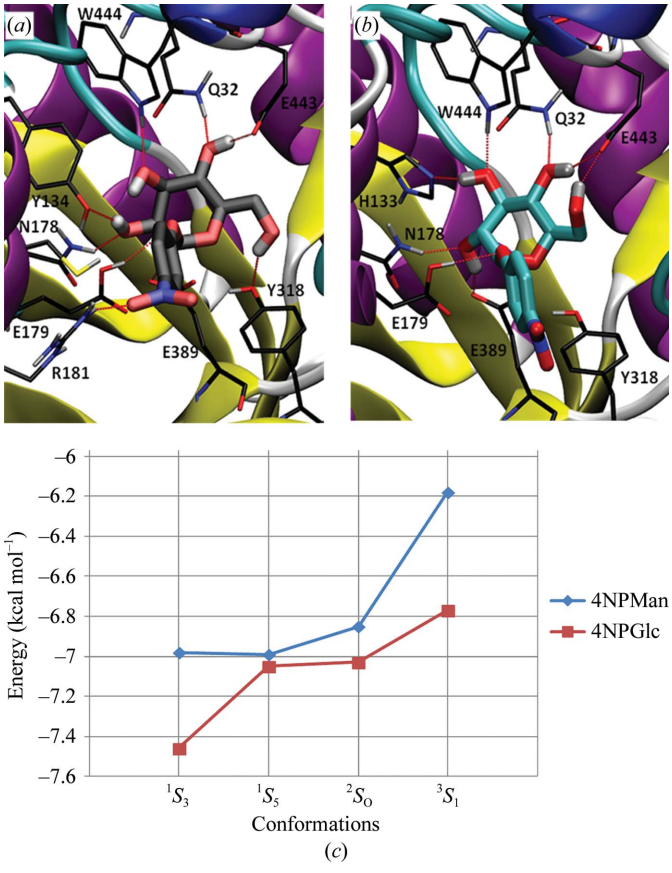

Figure 6
Structures of Os7BGlu26 in complex with 4NPGlc (*a*) and 4NPMan (*b*) obtained by docking. The distance between the carboxylic H atom of the catalytic acid/base residue (Glu179) and the glycosidic O atom is 3.08 Å for the glucoside and 3.58 Å for the mannoside. The distance between the $O^{\varepsilon1}$ atom of the nucleophile (Glu389) and the anomeric C atom is 2.98 Å for the glucoside and 3.0 Å for the mannoside. The binding energies of the different conformers of 4NPMan and 4NPGlc in complex with Os7BGlu26 are shown in (*c*).

Fig. 6 shows the enzyme complexes with the $^1S_5$ β-D-mannoside (4NPMan) and the $^1S_3$ β-D-glucoside (4NPGlc). The substrate is nicely accommodated in the binding cavity in each case. The mannose molecule forms hydrogen bonds to Gln32, Tyr134, Asn178, Glu179, Arg181, Tyr318, Glu443 and Trp444 (Fig. 6*b*) and the glucose molecule is hydrogen-bonded to Gln32, His133, Asn178, Glu179, Glu443 and Trp444 (Fig. 6*a*). The catalytic residues (Glu179 and Glu389) are well oriented for catalysis in both complexes (the carboxylic acid H atom of Glu179 points towards the glycosidic O atom and the nucleophile is within 3–3.5 Å distance of the anomeric C atom), in agreement with quantum-chemical studies of glycosidic bond hydrolysis (Petersen *et al.*, 2010; Biarnés *et al.*, 2011).

3.6. Comparison of Os7BGlu26 with covalent-intermediate complexes of other GH1 enzymes

To learn more about the residues that affect the glycon specificity of Os7BGlu26, we endeavoured to produce a covalent intermediate complex, as was previously achieved for Os3BGlu7 (Chuenchor *et al.*, 2008). Attempts to soak the mechanism-based inhibitors 2,4-dinitrophenyl 2-deoxy-2-fluoroglucoside (dNPG2F) and 2,4-dinitrophenyl 2-deoxy-2-fluoromannoside (dNPM2F) into the Os7BGlu26 crystals resulted in the release of 2,4-dinitrophenolate ions, as judged by a yellow chromophore. However, no glycon density was observed in the active site with either ligand. Pretreatment of Os7BGlu26 with dNPG2F or dNPM2F in sodium acetate buffer pH 5.0 resulted in rapid hydrolysis, with negligible

inhibition of the enzyme, at concentrations that strongly inhibited other rice GH1 enzymes (data not shown). Although an $^{O}S_2$ skew-boat mannosyl covalent complex with a GH26 β-D-mannanase has been reported (Ducros *et al.*, 2002), no such structure has been reported in the GH1 family. Therefore, the free Os7BGlu26 structure was superposed with the rice GH1 structures in complex with a bound 2-deoxy-2-fluoroglucoside (G2F) moiety. This moiety occupies a low-energy $^{4}C_1$ chair conformation and is covalently bound to the catalytic nucleophile residue (Fig. 7). We conjectured that the glucoside and mannoside substrates are likely to bind in the same positions and in the same orientations in enzymes that belong to the same family, although the conformations of these sugars may differ, as reported by Kuntothom *et al.* (2010) and supported by the computational docking studies in the previous section.

The identities and placement of nearly all of the amino-acid residues in direct contact with glycons in subsite −1 are conserved in the structures of rice GH1 isoenzymes, including the Os7BGlu26–β-D-mannose complex structure and the complexes with 4NPGlc and 4NPMan generated by molecular docking. The one exception is a tyrosine residue that is found in all characterized plant GH1 enzymes with β-D-mannosidase activity, *i.e.* Tyr134 of Os7BGlu26, which corresponds to Tyr131 of Os3BGlu7 (Fig. 7*a*), to Tyr136 of barley HvBII, to Tyr136 of tomato LeMside and to Tyr137 of *Arabidopsis* AtBGLU44. This tyrosine residue is substituted by tryptophan in Os3BGlu6 (Trp133) and Os4BGlu12 (Trp134), which lack β-D-mannosidase activity (Figs. 2 and 7*b*; Seshadri *et al.*, 2009; Opassiri *et al.*, 2010), and most other plant β-D-glucosidases, including all others with known crystallographic structures, although a few others have tyrosine, phenylalanine or smaller residues in this position (data not shown). It is noteworthy that this tyrosine residue makes a very close contact through a hydrogen bond with the catalytic acid/base residue. Inspection of the superimposed structures revealed that the acid/base residues of Os3BGlu6 and Os4BGlu12 are displaced slightly from the positions of the acid/base residues in Os3BGlu7 and Os7BGlu26 to form contacts through hydrogen bonds with Thr181 of Os3BGlu6 and Thr182 of Os4BGlu12 in the +1 subsite, whereas Os7BGlu26 and Os3BGlu7 have Cys182 and Ile179, respectively, in the corresponding positions. The equivalent residues from barley HvBII, tomato LeMside and *Arabidopsis* AtBGLU44, Val184, Val184 and Val185, respectively, do not have polar groups to form contacts through hydrogen bonds to the catalytic acid/base residue. Although this position is not unique in plant GH1 enzymes, most of those with known structures have threonine in this position, including maize Glu1, sorghum Dhr1, wheat and rye benzoxazinone glucoside β-D-glucosidases and *Rauvolfia serpentina* strictosidine and raucafricine β-D-glucosidases. White clover cyanogenic β-D-glucosidase (PDB entry 1cbg; Barrett *et al.*, 1995) has glycine in this position, but its catalytic acid/base residue maintains a position similar to those of Os3BGlu6, Os4BGlu12 and the other β-D-glucosidase structures with threonine in this position. Aside from the two differences noted above, the −1 subsite architecture is similar in the four rice GH1 structures. Therefore, amino-acid residues in other subsites or in the surrounding layers of residues outside catalytic sites might be important for the glycon specificity. Mutations of residues in the layers surrounding the active-site residues have been shown to modulate β-D-fucosidase *versus* β-D-glucosidase activities in an insect GH1 β-D-glucosidase (Mendonça & Marana, 2011). A recent attempt to increase the β-D-mannosidase activity of a plant β-D-glucosidase by mutagenesis of residues that were apparently close to the glycon in a homology model showed only marginal increases in the ratios of k_{cat}/K_m for 4NPMan *versus* 4NPGlc, leading the authors to similarly speculate that the shape of the active site may be more critical than the residues that directly interact with the glycon (Ratananikom *et al.*, 2013).

3.7. Kinetic studies of glycon-specificity mutants of Os7BGlu26

To investigate the function of the catalytic acid/base Glu179 and other key residues in the structure of Os7BGlu26 that

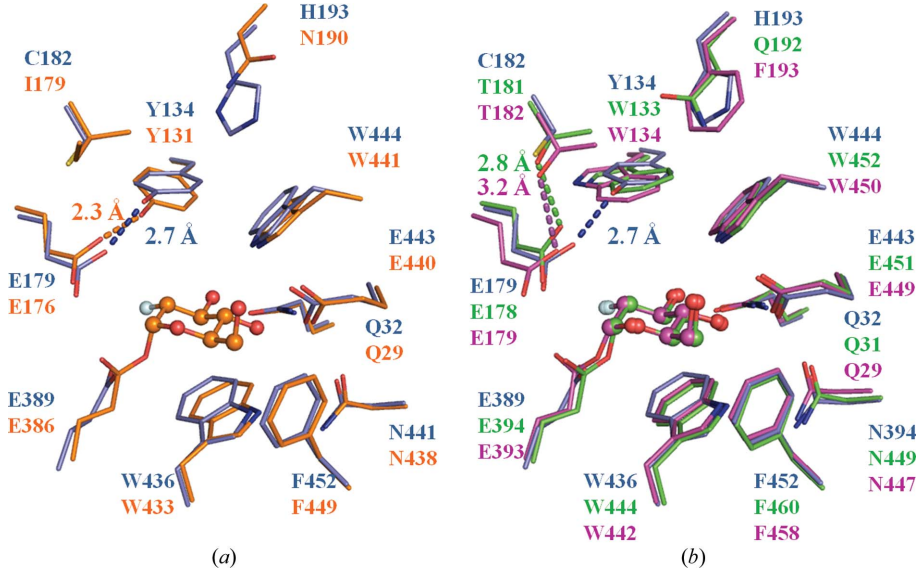

Figure 7
Comparison of the active sites of the rice Os7BGlu26 β-D-mannosidase and other rice GH1 β-D-glucosidases with bound 2-deoxy-2-fluoroglucoside (G2F) moieties. (*a*) Superimposition of Os7BGlu26 with Os3BGlu7 (PDB entry 2rgm), both of which have significant β-D-mannosidase activity. (*b*) Superimposition of Os7BGlu26 with Os3BGlu6 (PDB entry 3gnr) and Os4BGlu12 (PDB entry 3ptm), which do not have significant β-D-mannosidase activity, in complex with G2F. The structures are shown in stick representations, with C atoms coloured blue in Os7BGlu26, orange in Os3BGlu7, green in Os3BGlu6 and magenta in Os4BGlu12. The inhibitors are presented in ball-and-stick representations in the same colours as the corresponding protein.

were adjudged to play possible roles in Os7BGlu26 glycon specificity (*cf.* §3.6), we mutated Glu179 to Gln (E179Q), Tyr134 to Trp (Y134W), Tyr134 to Phe (Y134F), Cys182 to Thr (C182T) and Cys182 to Ala (C182A). We have also evaluated the effects of the Y134W, Y134F, E179Q, C182T and Y134W/C182T mutations on the hydrolysis of the β-D-glucoside and β-D-mannoside substrates in precise kinetic terms. The kinetic parameters and the Gibbs free-energy changes for the Os7BGlu26 mutations are presented in Table 2.

The Os7BGlu26 catalytic acid/base mutant E179Q showed lower activity than the wild type, as indicated by the low k_{cat}/K_m for both 4NPMan and 4NPGlc. However, this mutant affected the β-D-mannosidase activity more than the β-D-glucosidase activity: $\Delta\Delta G$ for 4NPMan was +9.0 kJ mol^{-1}, whereas $\Delta\Delta G$ for 4NPGlc was +8.1 kJ mol^{-1}. This change was driven by the 44-fold reduction in k_{cat} with little change in K_m for 4NPMan, although the K_m value increased eightfold and k_{cat} decreased nearly threefold for 4NPGlc. It should be noted that mutations of the catalytic acid/base to glutamine have been shown to have relatively high activity for substrates with good leaving groups, such as 4NP or 2,4-dinitrophenolate, which have low pK_a and have less need for protonation by the catalytic acid/base (Müllegger *et al.*, 2005; Chuenchor *et al.*, 2011). The use of acetate buffer, which can act as a substitute base or nucleophile, facilitates the deglycosylation step, so that this mutation has relatively mild effects in this assay. On the other hand, the mutation of Glu179 to alanine resulted in poor yields of soluble protein in this expression system, so this mutant could not be characterized (data not shown).

The Os7BGlu26 Y134W mutant had a lesser effect on the β-mannosidase activity (Table 2), as characterized by a $\Delta\Delta G$ of −0.9 kJ mol^{-1}. However, it showed a nearly sixfold increase in K_m to 2.37 m*M*, which was compensated by a nearly sevenfold increase in k_{cat} to 2.4 s^{-1}. Since this mutant caused a nearly fourfold decrease in K_m and little change in k_{cat} for 4NPGlc, it appeared to improve the binding of 4NPGlc and the transition state of the first covalent step of its hydrolysis (as judged by the $\Delta\Delta G$ of −3.5 kJ mol^{-1}). It is of note that the k_{cat}/K_m values of the Os7BGlu26 Y134W mutant for 4NPGlc and 4NPMan are nearly equal, although it still hydrolyzes 4NPMan much faster than 4NPGlc at substrate concentrations of above 0.01 m*M*. For Os7BGlu26 C182T, the K_m of the mutant was increased by approximately 25-fold to 30-fold for both substrates, but the k_{cat} increased 2.6-fold for 4NPGlc *versus* only 1.45-fold for 4NPMan. For this reason, the $\Delta\Delta G$ values were +7.1 and +6.2 kJ mol^{-1} for 4NPMan and 4NPGlc, respectively. To verify whether these changes were owing to the introduction of the hydrogen-bonding threonine or simply to removal of the cysteine sulfhydryl group, we also mutated Cys182 to alanine. The C182A mutation had minor effects on both 4NPMan ($\Delta\Delta G$ of +1.4 kJ mol^{-1}) and 4NPGlc ($\Delta\Delta G$ of +0.8 kJ mol^{-1}), suggesting that the major effect of the C182T mutation was from the introduction of the Thr182 side chain, which could hydrogen-bond to the catalytic acid/base. The double mutant Os7BGlu26 Y134W/C182T had kinetic parameters and $\Delta\Delta G$ similar to those of the single mutant C186T for 4NPGlc and the K_m value for 4NPMan was also similar to that of Os7BGlu26 C186T, but the k_{cat} was 40% lower for the double mutant. Hence, Y134W and C182T combined to give non-additive effects with 4NPMan ($\Delta\Delta G$ of +8.3 kJ mol^{-1}), which could be attributed to the fact that both mutated residues affect the position of the catalytic acid/base (Mildvan *et al.*, 1992; Mildvan, 2004). The results of our mutagenesis imply that the hydrogen bonding of neighbouring residues to the catalytic acid/base has a significant effect on the relative hydrolytic rates of β-D-mannoside *versus* β-D-glucoside substrates.

To differentiate whether the effect of the Y134W mutation was owing to the increase in size of the aromatic group or the loss of the hydrogen bond from the hydroxyl group to the catalytic acid/base, Tyr134 was mutated to Phe instead of Trp in Os7BGlu26 Y134F. The Y134F mutant showed a similar K_m to the wild-type enzyme for 4NPMan and a 1.4-fold increase in the K_m for 4NPGlc compared with the wild-type enzyme. Since the k_{cat} value was 4.4-fold that of the wild type for 4NPGlc, the k_{cat}/K_m of this mutant increased threefold to give a $\Delta\Delta G$ of −2.9 kJ mol^{-1}, which is a slightly smaller change than that observed for the Y134W mutant. However, the k_{cat} value for 4NPMan increased 36-fold and k_{cat}/K_m increased 39-fold compared with the wild-type enzyme to give a $\Delta\Delta G$ value of −9.2 kJ mol^{-1} for 4NPMan. Thus, the selectivity of this mutant for 4NPMan over 4NPGlc is improved more than 37-fold in terms of the relative k_{cat}/K_m values, suggesting that the smaller steric bulk of the aromatic residue is a critical factor in the preference for β-mannosidase over β-glucosidase substrates.

In summary, the determination of the structure of a plant GH1 β-D-mannosidase, Os7BGlu26, and structural investigations of the residues interacting with the glucoside or mannoside substrates indicated that the shape of the active site and the interactions with surrounding residues are critical for glycon specificity. The mutations described here had differential effects on the k_{cat}/K_m values of 4NPMan *versus* 4NPGlc, indicating that the residues interacting with the catalytic acid/base play a role in determining which of these is hydrolyzed more rapidly. Future structural and enzyme-kinetics studies of binding of substrate and transition-state analogues will be useful to further illuminate the interactions that differentiate the β-D-mannosidase and β-D-glucosidase activities in GH1.

We thank Professor Stephen Withers from the University of British Columbia for providing 2,4-dinitrophenyl 2-deoxy-2-fluoromannoside. We are also grateful to the Synchrotron Light Research Institute (SLRI) for providing reagents for crystal screening. This work was supported by the Thailand Research Fund Grant BRG5380017, the Strategic Scholarships for Frontier Research Network PhD Program and the National Research University Project to Suranaree University of Technology from the Commission on Higher Education of Thailand. RCR thanks the Agency for Science, Technology and Research (A*STAR), Singapore for support. Data collection was carried out at the National Synchrotron Radiation Research Center (NSRRC), a national user facility

supported by the National Science Council of Taiwan, ROC. The Synchrotron Radiation Protein Crystallography Facility is supported by the National Research Program for Genomic Medicine.

References

Ardèvol, A., Biarnés, X., Planas, A. & Rovira, C. (2010). *J. Am. Chem. Soc.* **132**, 16058–16065.

Barrett, T., Suresh, C. G., Tolley, S. P., Dodson, E. J. & Hughes, M. A. (1995). *Structure*, **3**, 951–960.

Biarnés, X., Ardèvol, A., Iglesias-Fernández, J., Planas, A. & Rovira, C. (2011). *J. Am. Chem. Soc.* **133**, 20301–20309.

Biarnés, X., Ardèvol, A., Planas, A., Rovira, C., Laio, A. & Parrinello, M. (2007). *J. Am. Chem. Soc.* **129**, 10686–10693.

Cantarel, B. L., Coutinho, P. M., Rancurel, C., Bernard, T., Lombard, V. & Henrissat, B. (2009). *Nucleic Acids Res.* **37**, D233–D238.

Chen, V. B., Arendall, W. B., Headd, J. J., Keedy, D. A., Immormino, R. M., Kapral, G. J., Murray, L. W., Richardson, J. S. & Richardson, D. C. (2010). *Acta Cryst.* D**66**, 12–21.

Chuenchor, W., Pengthaisong, S., Robinson, R. C., Yuvaniyama, J., Oonanant, W., Bevan, D. R., Esen, A., Chen, C.-J., Opassiri, R., Svasti, J. & Ketudat Cairns, J. R. (2008). *J. Mol. Biol.* **377**, 1200–1215.

Chuenchor, W., Pengthaisong, S., Robinson, R. C., Yuvaniyama, J., Svasti, J. & Ketudat Cairns, J. R. (2011). *J. Struct. Biol.* **173**, 169–179.

Czjzek, M., Cicek, M., Zamboni, V., Bevan, D. R., Henrissat, B. & Esen, A. (2000). *Proc. Natl Acad. Sci. USA*, **97**, 13555–13560.

Davies, G. J., Ducros, V. M., Varrot, A. & Zechel, D. L. (2003). *Biochem. Soc. Trans.* **31**, 523–526.

Davies, G. J., Mackenzie, L., Varrot, A., Dauter, M., Brzozowski, A. M., Schülein, M. & Withers, S. G. (1998). *Biochemistry*, **37**, 11707–11713.

Davies, G. J., Planas, A. & Rovira, C. (2012). *Acc. Chem. Res.* **45**, 308–316.

Dias, F. M., Vincent, F., Pell, G., Prates, J. A., Centeno, M. S., Tailford, L. E., Ferreira, L. M., Fontes, C. M., Davies, G. J. & Gilbert, H. J. (2004). *J. Biol. Chem.* **279**, 25517–25526.

Ducros, V. M., Zechel, D. L., Murshudov, G. N., Gilbert, H. J., Szabó, L., Stoll, D., Withers, S. G. & Davies, G. J. (2002). *Angew. Chem. Int. Ed. Engl.* **4**, 2824–2827.

Emsley, P. & Cowtan, K. (2004). *Acta Cryst.* D**60**, 2126–2132.

Fersht, A. R., Leatherbarrow, R. J. & Wells, T. N. (1987). *Biochemistry*, **26**, 6030–6038.

Gouet, P., Robert, X. & Courcelle, E. (2003). *Nucleic Acids Res.* **31**, 3320–3323.

Henrissat, B., Callebaut, I., Fabrega, S., Lehn, P., Mornon, J.-P. & Davies, G. (1995). *Proc. Natl Acad. Sci. USA*, **92**, 7090–7094.

Hommalai, G., Withers, S. G., Chuenchor, W., Ketudat Cairns, J. R. & Svasti, J. (2007). *Glycobiology*, **17**, 744–753.

Hrmova, M., Burton, R. A., Biely, P., Lahnstein, J. & Fincher, G. B. (2006). *Biochem. J.* **399**, 77–90.

Hrmova, M., Harvey, A. J., Wang, J., Shirley, N. J., Jones, G. P., Stone, B. A., Høj, P. B. & Fincher, G. B. (1996). *J. Biol. Chem.* **271**, 5277–5286.

Hrmova, M., MacGregor, E. A., Biely, P., Stewart, R. J. & Fincher, G. B. (1998). *J. Biol. Chem.* **273**, 11134–11143.

Jeng, W.-Y., Wang, N.-C., Lin, M.-H., Lin, C.-T., Liaw, Y.-C., Chang, W.-J., Liu, C.-I., Liang, P.-H. & Wang, A. H.-J. (2011). *J. Struct. Biol.* **173**, 46–56.

Jenkins, J., Lo Leggio, L., Harris, G. & Pickersgill, R. (1995). *FEBS Lett.* **362**, 281–285.

Kuntothom, T., Luang, S., Harvey, A. J., Fincher, G. B., Opassiri, R., Hrmova, M. & Ketudat Cairns, J. R. (2009). *Arch. Biochem. Biophys.* **491**, 85–95.

Kuntothom, T., Raab, M., Tvaroska, I., Fort, S., Pengthaisong, S., Cañada, J., Calle, L., Jiménez-Barbero, J., Ketudat Cairns, J. R. & Hrmova, M. (2010). *Biochemistry*, **49**, 8779–8793.

Laskowski, R. A., MacArthur, M. W., Moss, D. S. & Thornton, J. M. (1993). *J. Appl. Cryst.* **26**, 283–291.

Matthews, B. W. (1968). *J. Mol. Biol.* **33**, 491–497.

McCleary, B. & Matheson, N. (1975). *Phytochemistry*, **14**, 1187–1194.

Mendonça, L. M. & Marana, S. R. (2011). *Biochim. Biophys. Acta*, **1814**, 1616–1623.

Mildvan, A. S. (2004). *Biochemistry*, **43**, 14517–14520.

Mildvan, A. S., Weber, D. J. & Kuliopulos, A. (1992). *Arch. Biochem. Biophys.* **294**, 327–340.

Mo, B. & Bewley, J. D. (2002). *Planta*, **215**, 141–152.

Morris, G. M., Huey, R., Lindstrom, W., Sanner, M. F., Belew, R. K., Goodsell, D. S. & Olson, A. J. (2009). *J. Comput. Chem.* **16**, 2785–2791.

Müllegger, J., Jahn, M., Chen, H.-M., Warren, R. A. J. & Withers, S. G. (2005). *Protein Eng. Des. Sel.* **18**, 33–40.

Murshudov, G. N., Skubák, P., Lebedev, A. A., Pannu, N. S., Steiner, R. A., Nicholls, R. A., Winn, M. D., Long, F. & Vagin, A. A. (2011). *Acta Cryst.* D**67**, 355–367.

Offen, W. A., Zechel, D. L., Withers, S. G., Gilbert, H. J. & Davies, G. J. (2009). *Chem. Commun.*, pp. 2484–2486.

Opassiri, R., Hua, Y., Wara-Aswapati, O., Akiyama, T., Svasti, J., Esen, A. & Ketudat Cairns, J. R. (2004). *Biochem. J.* **379**, 125–131.

Opassiri, R., Maneesan, J., Akiyama, T., Pomthong, B., Jin, S., Kimura, A. & Ketudat Cairns, J. R. (2010). *Plant Sci.* **179**, 273–280.

Opassiri, R., Pomthong, B., Onkoksoong, T., Akiyama, T., Esen, A. & Ketudat Cairns, J. R. (2006). *BMC Plant Biol.* **6**, 33.

Otwinowski, Z. & Minor, W. (1997). *Methods Enzymol.* **276**, 307–326.

Ouellette, B. F. F. & Bewley, J. D. (1986). *Planta*, **169**, 333–338.

Petersen, L., Ardèvol, A., Rovira, C. & Reilly, P. J. (2010). *J. Am. Chem. Soc.* **132**, 8291–8300.

Ratananikom, K., Choengpanya, K., Tongtubtim, N., Charoenrat, T., Withers, S. G. & Kongsaeree, P. T. (2013). *Carbohydr. Res.* **373**, 35–41.

Rye, C. S. & Withers, S. G. (2000). *Curr. Opin. Chem. Biol.* **5**, 573–580.

Sansenya, S., Opassiri, R., Kuaprasert, B., Chen, C.-J. & Ketudat Cairns, J. R. (2011). *Arch. Biochem. Biophys.* **510**, 62–72.

Sanz-Aparicio, J., Hermoso, J. A., Martínez-Ripoll, M., Lequerica, J. L. & Polaina, J. (1998). *J. Mol. Biol.* **275**, 491–502.

Seshadri, S., Akiyama, T., Opassiri, R., Kuaprasert, B. & Ketudat Cairns, J. (2009). *Plant Physiol.* **151**, 47–58.

Tailford, L. E., Offen, W. A., Smith, N. L., Dumon, C., Morland, C., Gratien, J., Heck, M.-P., Stick, R. V., Blériot, Y., Vasella, A., Gilbert, H. J. & Davies, G. J. (2008). *Nature Chem. Biol.* **4**, 306–312.

Vagin, A. & Teplyakov, A. (2010). *Acta Cryst.* D**66**, 22–25.

Verdoucq, L., Morinière, J., Bevan, D. R., Esen, A., Vasella, A., Henrissat, B. & Czjze, M. (2004). *J. Biol. Chem.* **279**, 31796–31803.

Vocadlo, D. J. & Davies, G. J. (2008). *Curr. Opin. Chem. Biol.* **12**, 539–555.

Winn, M. D. *et al.* (2011). *Acta Cryst.* D**67**, 235–242.

Xu, Z., Escamilla-Treviño, L., Zeng, L., Lalgondar, M., Bevan, D., Winkel, B., Mohamed, A., Cheng, C.-L., Shih, M.-C., Poulton, J. & Esen, A. (2004). *Plant Mol. Biol.* **55**, 343–367.